Precision & Performance Conference 2025, Cranfield University, UK, 17th- 20th November 2025

Experimental characterization of thermal disturbances in a 6DOF nanopositioning system under varying operational conditions

Parastoo Salimitari[1], Steffen Hesse[1], Michael Katzschmann[1], Ludwig Herzog[1]

[1] *IMMS Institut für Mikroelektronik- und Mechatronik-Systeme gemeinnützige GmbH (IMMS GmbH)*

Parastoo.salimitari@imms.de

Abstract

Thermal stability is critical to the precision and performance of nanopositioning systems (NPS). This paper experimentally investigates thermal disturbances within a 6 degree of freedom (6DOF) NPS using a targeted temperature sensor placement strategy. Temperature data over time are recorded and analyzed under typical operational conditions to study thermal behavior across different system components. This enables the identification of key elements with primary contribution to thermal drift. Findings from this study can provide insight into thermal management strategies for improving the accuracy and long-term reliability of nanopositioning systems.

Nanopositioning system, thermal disturbance, thermal management strategies

1. Introduction

NPSs are vital tools in fields requiring extreme precision, such as nanotechnology, scanning probe microscopy and optical metrology [1], [2]. These systems, however, are highly sensitive to environmental factors, among which thermal disturbances play a critical role. Temperature variations cause mechanical expansion or contraction, leading to thermal drift and positioning instability [3]. Despite careful mechanical design, thermal effects remain a limiting factor in long-term system performance.

Several previous studies have addressed thermal stability in precision systems. While these contributions have advanced the field by exploring low thermal expansion materials or introducing active thermal compensation algorithms for drift correction [4], [5], many rely on specialized system designs or assume ideal laboratory conditions that are not representative of typical industrial environments [3].

In contrast, this research systematically records and analyzes the thermal behavior of an NPS during typical operational conditions without special environmental control. The goal is to investigate the practical thermal response of various components and identify the sources most responsible for thermal drift. Temperature data is recorded over time and visualized to examine the dynamic thermal behavior across the system and determine the dominant heat contributors.

This paper is organized as follows: Section 2 describes the data acquisition methodology. Section 3 outlines the system configuration and identifies key heat sources. Section 4 analyzes the thermal behavior of subsystems under various operating conditions. Section 5 summarizes the findings and proposes strategies for thermal drift reduction.

2. Methodology

To investigate thermal disturbances within an NPS, naming NPS6D200, a systematic data collection approach was implemented. Thin film NTC thermistors were placed at 23 key locations. The thermistor specifications and image are shown in Figure 1. Each sensor was individually calibrated, and the resulting calibration curves were used to generate fit functions that convert resistance values into accurate temperature readings.

Measurements were conducted over multiple sessions lasting from a few hours up to 70 hours, during which the system operated under standard laboratory conditions (ambient temperature 22 ± 1°C). Graphical visualizations were generated using MATLAB, providing time-series graphs and comparative plots across components. For all experiments, the system housing remained closed to minimize the effect of external disturbances.

No-load resistance at 25 ˚C	10000 Ω
Tolerance at 25 ˚C	± 1%
Beta (25/85) Constant	3435 K ± 1%
Operating temperature range	-30 ˚C - 120 ˚C

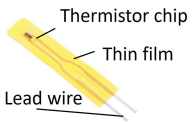

Figure 1. Thin Film NTC Thermistor specifications and image.

3. Heating sources in the NPS6D200 tool

The system under study is a 6D closed-loop control positioning system which provides full six-axis motion (x, y, z, ϕ_x, ϕ_y, ϕ_z) via planar motor, vertical actuators and aerostatic guidance, shown in Figure 2. The long-range motion of the system in 3D is provided by moving permanent magnets placed on a slider and three linear drive units which are supported on a granite base. Each drive unit consists of a pair of flat coils encapsulated in stainless steel heat exchangers with internal water cooling on both sides of the coils. The three drive units are arranged with 120° angle to provide the force in any direction within the xy-plane and they act simultaneously without contacting the slider. The slider is supported above the base plate by three lifting and actuation units (LAUs) providing a planar air-bearing at the bottom of each LAU, enabling frictionless motion within a diameter of 200 mm. A

vertical displacement of up to 25 mm is integrated into the system using coil lift units (CLUs) that move the common base of the drive units with respect to the *z*-position of the slider. The lifting units (i.e., CLUs and LAUs) are supplied with compressed air, while the exhaust air is drained so that it does not escape into the environment.

The movement of the slider in *x*, *y* and ϕ_z is measured using three high-resolution laser interferometers (U, V, W) and is controlled in closed loop with sub-nm servo error. On the other hand, *z*, ϕ_x and ϕ_y movement is measured by the vertical laser interferometer (Z) and an autocollimator angle sensor installed below the center of the slider. The measuring units are fixed while the sample can be moved in different directions. The interferometer axes are arranged to always intersect at the touching point of the sample over the entire range of movement to fulfill the Abbe principle. Detailed explanation of the setup can be found elsewhere [6].

Although the NPS6D200 is enclosed in a thermal and acoustic housing constructed with multi-layer foam to reduce external temperature and sound disturbances, internal heat sources cause noticeable temperature gradients. Since different components affect the system's thermal drift differently, a targeted temperature sensor placement strategy was applied. Sensor locations include:

- Four sensors per coil unit: two on coils, two at the water-cooling inlet/outlet but not in the water flow (A, B, and C – yellow circles in Figure 2)
- One sensor per LAU (1, 2, 3 – blue circles)
- One sensor near laser interferometer (LIF) beam paths of W and Z – green circles
- One sensor on the Laser Focus Sensor (LFS) mounting part
- One sensor on the outer housing wall
- Four sensors in the air supply and drain lines for LAUs and CLUs

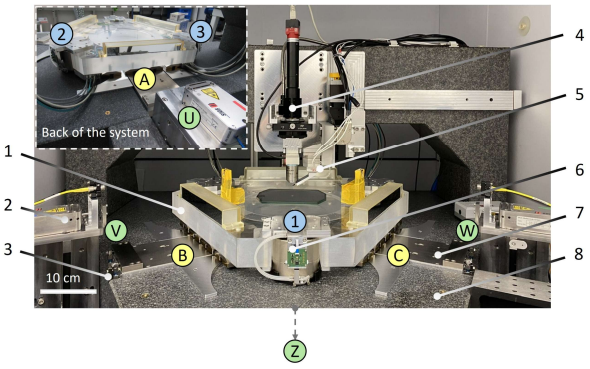

Figure 2. Photograph of NPS6D200 containing: 1) slider with reflectors, 2) LIFs naming U, V, W and Z in green circles (Z is placed vertically below the center of slider), 3) CLUs, 4) mounted analysis tool, here LFS, 5) mounted AFM system, 6)LAUs naming 1, 2 and 3 in blue circles 7) coil units of the planar direct drive naming A, B and C in yellow circles and 8) granite base. The inset on the left side shows the back view of the system.

4. Temperature analysis

The objective of this research is to investigate, through experimentation, the thermal contribution of key components which can facilitate heat removal or temperature control of the system. Therefore, the thermal effects of various active components were systematically analyzed under different operating modes. One representative experiment is summarized in the following table and the result is shown in Figure 3 (a). This experiment was conducted over 22 hours while the system was powered and in closed-loop controlled standstill throughout the experiment.

Experiment 1 for 22 h			
Coils	LAUs	LIFs	LFS
ON	ON	ON	ON

A static temperature difference of approximately 0.5 °C was observed between the top and bottom of the granite base by comparing LIF_W and LIF_Z. Among all monitored components, the LFS exhibited the greatest temperature rise, showing a differential of about 1 to 1.5 °C relative to other component's temperature.

To better illustrate the influence of LFS heating on nearby components, in a separate experiment conducted for 70 hours, the LFS and LIF were turned off after about 20 hours. The stage and controller remained off throughout the experiment.

Experiment 2 for 70 h			
Coils	LAUs	LIFs	LFS
OFF	OFF	ON $\xrightarrow{20\,h}$ OFF	ON $\xrightarrow{20\,h}$ OFF

As seen in Figure 3 (b), the temperature curves of other components closely follow the LFS temperature, suggesting strong thermal coupling between the LFS and neighboring subsystems. It was also observed in Figure 3 (b) that when the stage is off, i.e., no air flows through the LAUs and CLUs, similar temperatures are recorded in LAUs and coils (~ 20 °C), suggesting passive thermal equilibrium. In contrast, active heating from the drive coils during operation can transfer heat into the granite base, inducing structural deformation. The following sections examine the main sources of heat in more detail.

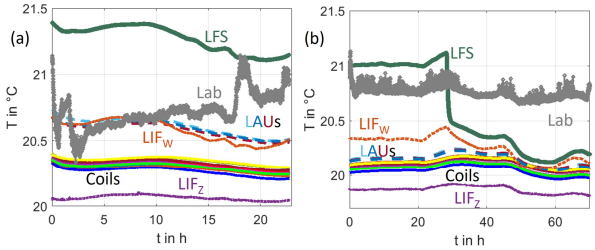

Figure 3. Temperature measurement in °C over time in h for (a) experiment 1 and (b) experiment 2.

4.1. Temperature analysis of mounted analysis tool

A mounted analysis tool can be a key source for thermal drift since they generate localized heat during operation which is typically not evenly distributed because of their electronics, lasers or materials. To evaluate the thermal effect of such a mounted analysis tool, here an LFS, further experiments were designed in which only the heat generation of the LFS was considered while other factors were removed. For this purpose, the LFS was placed inside a self-fabricated isolation box (Figure 4(a)) with a volume of 25 x 38 x 16 cm^3 made of acoustic foam with a thickness of 4 cm. To improve the measurement of the heat generated by the LFS and reduce the effect of the surrounding environment, the temperature sensor was glued to the main body near the electronic unit by copper tape and fixed by another polyimide tape as shown in the inset of Figure 4(a). To measure the temperature of the air inside the box as well as the lab temperature, four sensors were placed inside the box and one sensor outside. The experiment was performed for 24 hours and the LFS was turned on after 2 hours (green vertical line in Figure 4 (b)) and turned off after 19 hours (red vertical line).

As it can be seen in Figure 4(b), when the LFS is powered, the temperature measured by the attached sensor (green graph) shows a sharp 1 °C increase in the first 1 hour. By considering the volume of the isolation box, V = 0.0152 m^3, density of air,

ρ = 1.2 kg/m^3, and specific heat capacity of air, c = 1005 J/kgK, the heat rate of the LFS in the first hour after turning ON can be calculated:

$$\frac{Q}{t} \cong mc\frac{\Delta T}{t} \cong \rho V c\frac{\Delta T}{t} \cong 5\ mW$$

The temperature increase is followed by a slower increase of 1 °C in the remaining 18 hours. A similar trend was observed in the surrounding air inside the box, confirming a measurable temperature increase in the box due to LFS heating.

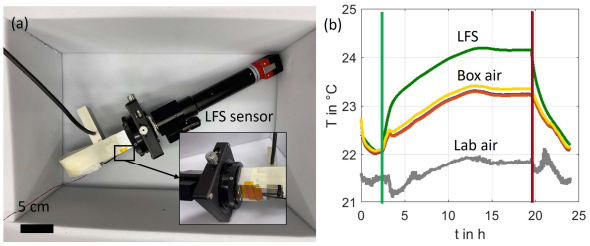

Figure 4. (a) Photograph of the LFS inside the self-made isolation box and (b) the resulting graph of experiment 3.

This experiment confirms that a mounted analysis tool, independent of any interaction with other active components, is a significant source of thermal disturbances. Its local heating creates strong thermal gradients that can propagate through mechanical structures, resulting in positioning drift.

4.2. Temperature analysis of coil units

The coil units are another important heat source because they actively generate heat during operation which can also lead to localized heating. In the NPS6D200, they are almost not in direct mechanical contact with the granite base of the system, but they can induce heat into other components which can potentially influence the stability and precision of the system. As mentioned earlier, coil units are embedded in stainless steel housing with internal tempering channels. A thermostat and a water cycle are intended to maintain the desired water temperature for active cooling. However, to better investigate the thermal behavior of the compressed air or active components (e.g., coils, LFS) and minimizing the heat transfer into the flowing medium, the water cycle system is not activated in the experiments mentioned in this work, although cooling channels are already filled with water.

An experiment was conducted where the system is turned on after 1 hour (green vertical line in Figure 5) and turned off after 25 hours and 30 min (red vertical line in Figure 5). The results show that the coil temperature drops by about 0.2 °C after their activation and increased again after turning off the coils. By considering the fact that coils should produce heat after activation and the cooling channels are not circulating, the thermal behavior of the coils is strange. It should be noted that the observed temperature change is recorded by all sensors directly on the coils and at the water-cooling inlet/outlet which can be seen in magnified images (1) and (2) in Figure 5. The reason might be the air supplied to the lifting units when the stage is turned on leading to Joule-Thomson effect. Based on this effect, the temperature of a gas or liquid changes when it is expanding, typically because of the pressure loss from flowing through a valve. Since the air supplied to the respective air bearing of the lifting units flows through micro-nozzles, the air pressure is reduced from about 5 bar to the atmospheric pressure which results in temperature decrease of the air. After removing the air supply, the temperature will rise again, which is also noticeable in the LAUs graph in Figure 5. Although similar results were observed after repeating the experiment, more investigation is required to thoroughly understand the reason for this behavior.

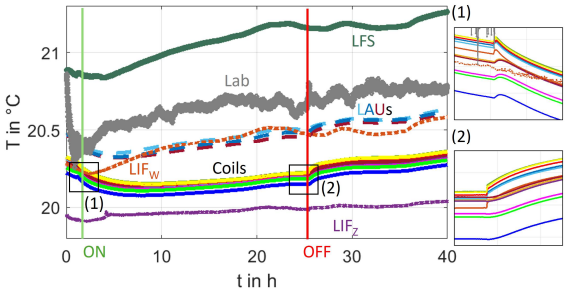

Figure 5. Temperature measurement over time for experiment 4.

4.3. Temperature analysis of supplied air into LAUs and CLUs

As mentioned in the previous section, the temperature of the compressed air supply and drain into LAUs and CLUs can play an important role in the thermal behavior of the system. Therefore, it is required to expand the analysis by monitoring the compressed air temperature using temperature sensors in the air supply and drain tubes. For this purpose, custom fittings were used to place the sensors in the air tubes having in-flow (T-shape) (Figure 6(a)) and retracted configurations (Figure 6(c)). The compressed air is supplied by the pneumatic supply unit (PSU) after powering the stage having the operating pressure of 4-6 bar and flow rate of 10 Nl/min (Normal liter per minute). Two representative experiments using these sensors are summarized in the following table.

Experiment 5 for 21 h (T-shape sensor)			
Coils	LAUs	LIFs	LFS
OFF $\xrightarrow{2\ h}$ ON $\xrightarrow{15\ h}$ OFF	OFF $\xrightarrow{2\ h}$ ON $\xrightarrow{15\ h}$ OFF	ON	ON
Experiment 6 for 60 h (retracted sensor)			
Coils	LAUs	LIFs	LFS
OFF $\xrightarrow{2\ h}$ ON	OFF $\xrightarrow{2\ h}$ ON	ON	ON

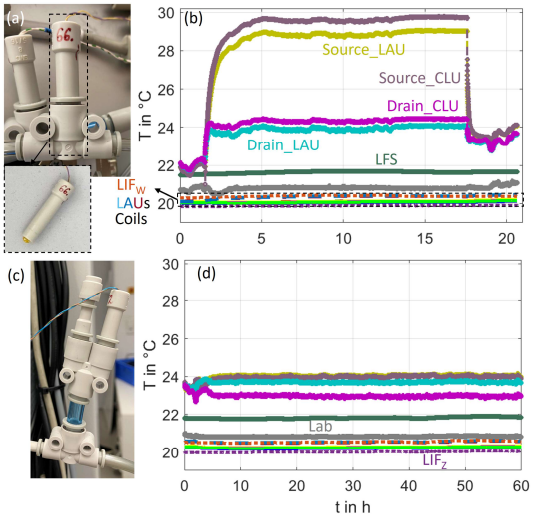

Figure 6. (a) Photograph of the sensor in the flow of the air supply (T-shape sensor) and (b) its corresponding graph for experiment 5. (c) Photograph of the sensor retracted from the flow of the air supply (retracted sensor) and (d) its corresponding graph for experiment 6.

In experiment 5, the Source_LAU and Source_CLU sensors in the air supply tubes recorded a temperature increase to about 29 °C after powering the stage, while Drain_LAU and Drain_CLU sensors in the drained air flow showed a smaller increase to about 24 °C. This suggests that the PSU is heating the incoming air, which subsequently loses heat to the system before exiting. After turning off the stage and consequently the PSU, supplied and drained air temperatures dropped

rapidly. In contrast, by using retracted sensors in experiment 6, little to no temperature change was observed after turning on the PSU, as seen in Figures 6(d).

Due to the huge difference between the temperature measured by these two types of sensors, it is required to analyze their performance separately while the influence of other factors is minimized. Moreover, since these sensors are outside the enclosure and near other modules, their heating source might be the surrounding environment.

Therefore, another experiment was designed in which the previously mentioned isolation box was used to place the sensors inside it. Two retracted sensors (1 and 2) and one T-shape sensors (5*) are installed in the air path from global supply while this air path is divided into two routes; one going to the PSU and the other is connected to an adjustable valve (q_s) to set the flow rate after passing a retracted sensor (3). Another tube is coming out of the PSU which goes through a retracted sensor 1 and a T-shape sensor 6* and connects to another adjustable valve (q_s). Sensor 7 is measuring the air inside the box and sensor 8 is allocated to the lab temperature. The experiment was performed for almost three days and is summarized in the following table.

Experiment 7 for 65 h		
First day	Second day	Third day
q_s : OFF PSU: ON (after 2 h)	q_s : ON (5.6 Nl/min) PSU: ON	q_s : ON (8.5 Nl/min) PSU: ON

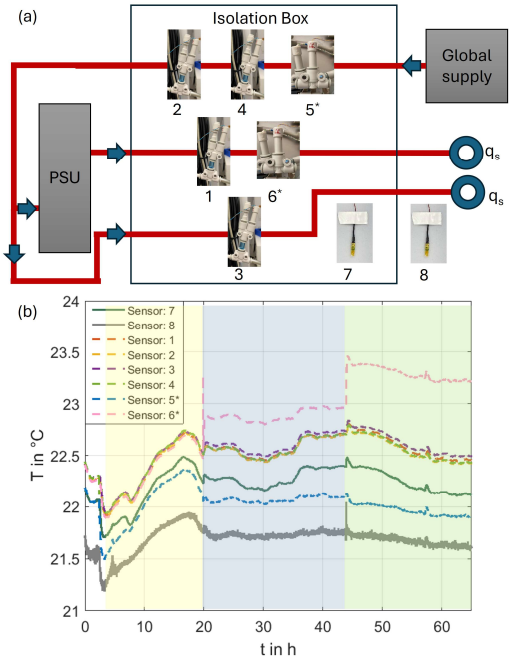

Figure 7. (a) Schematic illustration of sensors connection. (b) The corresponding graph of experiment 7.

Figure 7 shows the sensor layout and resulting graph of the experiment. When the PSU was turned on while airflow was off, sensor 5* recorded a temperature drop compared to the ambient (sensor 7), indicating cool air entering from the main supply (yellow region of Figure 7(b)). When air flow was set to 5.6 Nl/min by the adjustable valve (blue region), only sensor 6*, which was in the air stream, recorded an increase of 0.4 °C while other sensors were following the temperature graph of the ambient (sensor 7). This effect increased again during a high-flow phase of 8.5 Nl/min (green region), with an additional temperature rise of 0.4 °C.

These observations lead to the conclusions that only sensors exposed directly to the air stream can measure actual air temperature; retracted sensors are probably reflecting the fitting or surrounding temperatures. Additionally, the PSU heats the air by ~0.4 °C at 5.6 Nl/min and by an additional ~0.4 °C at higher flow of 8.5 Nl/min due to higher heat transfer from increased mass flow rate.

Accordingly, it seems that the results of experiment 5 which were recorded by T-shape sensors (Figure 6(b)) were reliable and the PSU is actually heating the air flow but reaching the temperature of about 29 °C can be due to closeness of these sensors to other modules. Therefore, one passive solution to reduce the air flow temperature before entering the enclosure and the system is to extend the length of tubes to cool the compressed air to laboratory temperature.

5. Conclusion

This study presents a detailed analysis of thermal disturbances in key components of a nanopositioning system under realistic operating conditions. Among all components, the mounted tool, which here is an LFS, is identified as the most significant internal heat source. Its continuous operation leads to strong thermal gradients that propagate through the mechanical structure, requiring active cooling or isolation. Drive units also contribute to internal heating which can be managed with an integrated water-cooling system. However, strange behavior is observed in the sensors on the coils and at the water-cooling inlet/outlet after turning on the stage which can be explained by the Joule-Thomson effect. In addition, the air supply for LAUs and CLUs introduces thermal disturbance, largely influenced by the PSU. This heat should be conditioned before entering the system, for example by integration of long tubes or an external thermal control unit. Considering the focus of this work to experimentally investigate thermal influence of the key active components and the compressed air supply, more systematic experimental and modelling analysis are required to propose heat regulation techniques.

Future work will focus on developing predictive compensation models using thermal sensor feedback, and on integrating temperature-dependent corrections into the control loop to minimize real-time drift.

Funding Info: The research group ‘Application of AI-based virtual sensor technology to effectively increase the precision of positioning systems – VirtuSen’ is funded by the German Land of Thüringen.

References

[1] Y. Chen, Z. Shu, S. Zhang, P. Zeng, H. Liang, M. Zheng, and H. Duan, “Sub-10 nm fabrication: methods and applications,” *International Journal of Extreme Manufacturing*, **vol. 3**, no. 3, p. 032002, Jul. 2021.

[2] J. Stauffenberg, I. Ortlepp, J. Belkner, D. Dontsov, E. Langlotz, S. Hesse, I. Rangelow, and E. Manske, “Measurement Precision of a Planar Nanopositioning Machine with a Range of Motion of Ø100 mm,” *Applied Sciences 2022, **Vol. 12**, Page 7843*, vol. 12, no. 15, p. 7843, Aug. 2022.

[3] J. Wang, C. Zhu, M. Feng, and W. Ren, “Thermal error modeling and compensation of long-travel nanopositioning stage,” *International Journal of Advanced Manufacturing Technology*, **vol. 65**, no. 1–4, pp. 443–450, Mar. 2013.

[4] P. Juasiripukdee, I. Maskery, I. Ashcroft, and R. Leach, “Low Thermal Expansion Machine Frame Designs Using Lattice Structures,” *Applied Sciences 2021, **Vol. 11**, Page 9135*, vol. 11, no. 19, p. 9135, Sep. 2021.

[5] Y. Jia, H. Tang, S. Xu, Y. Xu, X. Chen, and Y. Tian, “A Novel Decoupled Flexure Nanopositioner With Thermal Distortion Self-Elimination Function,” *IEEE/ASME Transactions on Mechatronics*, **vol. 27**, no. 5, pp. 2953–2962, Oct. 2022.

[6] S. Hesse, A. Huaman, M. Katzschmann, B. Leistritz, and L. Herzog, “NPS6D200—A Long Range Nanopositioning Stage with 6D Closed Loop Control,” *Applied Sciences (Switzerland)*, **vol. 14**, no. 16, Aug. 2024.